

Influence of finite-temperature effects on CMB power spectrum

I. Y. Park[†] and P. Y. Wui[♠]

[†]*Department of Applied Mathematics, Philander Smith University
Little Rock, AR 72202, USA
inyongpark05@gmail.com*

[♠]*Department of Business Administration, University of Arkansas at Pine Bluff
Pine Bluff, AR 71601, USA
wuiy@uapb.edu*

Abstract

We explore the implications of finite-temperature quantum field theory effects on cosmological parameters within the framework of the Λ CDM model and its modification. By incorporating temperature-dependent corrections to the cosmological constant, we extend the standard cosmological model to include additional density parameters, Ω_{Λ_2} and Ω_{Λ_3} , which arise from finite-T quantum gravitational effects. Using the Cosmic Linear Anisotropy Solving System, we analyze the impact of these corrections on the cosmic microwave background power spectrum and compare the results with the Planck 2018 data. Through brute-force parameter scans and advanced machine learning techniques, including quartic regression, we demonstrate that the inclusion of Ω_{Λ_2} and Ω_{Λ_3} improves the model's predictive accuracy, achieving high R^2 values and low mean squared error. The present work paves the way for future research into higher-order corrections and enhanced computational methods for cosmological parameter estimation.

1 Introduction

Understanding the cosmological parameters that govern the Universe is central to modern cosmology [1, 2], with models of cosmological parameter estimation evolving to incorporate increasingly sophisticated methods and data sources. Among the most influential studies, the Planck 2018 results [3] have provided a comprehensive analysis of cosmological parameters derived from CMB anisotropies, utilizing high-precision data to set a benchmark for subsequent analyses. These measurements impose stringent constraints on key parameters such as the density of different components of the Universe, the Hubble constant, and the spectral index. As a result, they have guided our understanding of the Universe’s composition and evolution, and provided a solid foundation for both theoretical models and observational research. However, while these results have enhanced our ability to probe the cosmological landscape, the models themselves are still evolving. For instance, there are ongoing efforts to refine the assumptions underlying the cosmological constant (CC) and the potential roles that quantum effects may play over cosmic time. While the conventional hydrodynamic approach incorporates temperature via classical thermodynamics, it is crucial to also consider the temperature effects from finite-temperature (finite-T) quantum field theory (QFT) (see [4] for a review), as recently elaborated in references [5] [6], and [7]. Given the high temperatures in the early Universe, these effects are unlikely to be disregarded when studying its history. This work aims to analyze the implications of a finite-T-corrected cosmological parameters in light of these considerations.

The conventional hydrodynamic approach as well as the one based on Boltzmann’s equations is essentially a classical framework: it does not take into account the quantum effects introduced by finite-T QFT. In addition to classical thermodynamics, finite-T QFT effects should play a significant role in the cosmological constant, feeding into it through perturbative quantum corrections. Ideally, a second-quantized description whose effective description is provided by the hydrodynamic should be employed. Imagine obtaining the quantum action, i.e., 1PI action. (Only the first several terms in the derivative expansion will matter.) The loop contributions to the CC depend on the temperature. This in turn implies that in the corresponding FLRW-type cosmology the CC comes to be time-dependent through the time-dependence of the temperature [7].¹ Finite-T effects were considered earlier [5] [6]² to tackle the long-standing cosmological constant problem. See [18], [19], and [20] for an inspiring review of the CC problem and subsequent works. The CC problem was originally observed from the technical feature of onshell renormalization that the one-loop correction is enormously larger than the observed value of the CC, which necessitated a fine-tuned cancellation between the renormalized value of the CC and the one-loop correction. However, what has been noted in [5–7] (see also [13] and [14]) was that if one takes the renormalized

¹A time-dependent CC implies the following for the conservation laws [7]. With separate conservation for matter and radiation, one does not impose its separate conservation condition for the CC. Instead, the conservation equation of the total stress tensor follows from the Einstein equation. This bears an interesting implication for renormalization of the Newton’s constant.

²These works are finite-temperature extensions of earlier works on foliation-based gravity quantization [8], with one key element being the physical state condition [9] (see [10] for a similar idea). In [11], the gauge $K = 0$ (more generally $K = K_0$), where K denotes the trace of the second fundamental form, was employed as a crucial ingredient for quantization. A similar approach was later applied in Witten’s recent work [12].

mass to be on the order of the temperature - which is hinted by the fact that the presence of temperature yields a T^4 -order CC term at the quantum level, the one-loop correction becomes small and this naturally allows one to take a small value of the renormalized value of the CC. It has been proposed that the CC problem may well be a matter of how to manage perturbation theory and finite renormalization, instead of a genuine problem. See also [21] for a recent related discussion.

We consider a temperature-dependent CC (and its implications for the other cosmological parameters) for several reasons. First, the temperature effects are unavoidable due to perturbative quantum gravitational influences, making it impossible to omit unless negligible. Since we're considering periods around or before recombination, these finite-T QFT effects are not negligible, though small, especially given the observed smallness of the present-day CC. Second, these effects exhibit the characteristics needed for early dark energy (see [22] for a review of early dark energy), making the temperature-dependent CC a form of early dark energy present throughout the Universe's history. Their contribution is significant in the radiation-dominant era and around last scattering.

At the phenomenological level, the crux of our approach is that the finite-T effects naturally introduce additional parameters with which to fit the data. It is not difficult to see how these extra parameter arises. As discussed in the body, the form of the CC after taking the leading finite-T quantum correction into account is $\Lambda = \Lambda_1 + \Lambda_2 \frac{1}{a^4} + \Lambda_3 \frac{1}{a^2} + \dots$ where a denotes the scale parameter; Λ_1, Λ_2 , and Λ_3 are genuine (viz., time-independent) constants. In view of this it is natural to introduce the corresponding density parameters $\Omega_{\Lambda_2}, \Omega_{\Lambda_3}$ in addition to Ω_{Λ_1} , the usual vacuum energy density parameter. (One may raise that the parameters Ω_{Λ_2} and Ω_{Λ_3} can be absorbed into the Ω_r and Ω_K , the radiation and curvature density parameters, respectively; see the discussion below for this.) At the early stage of the matter dominance, the Λ term, which is now temperature-dependent and scales as $\sim \frac{1}{a^4}$, is not negligible compared with the a^{-3} behavior of matter. In other words, the Λ term is a priori expected to make a non-negligible contribution to the Hubble constant between radiation dominance and radiation-matter equality, the period important for some early dark energy models. We thus consider extension of the original Λ CDM model by including Ω_{Λ_2} and Ω_{Λ_3} . For the actual analysis of the finite-T modified system, we employ the cosmic linear anisotropy solving system (CLASS) [15, 16].

More specifically we consider the model that has the following eight parameters, $(\Omega_{\Lambda_2}, \Omega_{\Lambda_3}, h, \omega_b, \omega_{cdm}, A_s, n_s, \tau_{reio})$ [17], and compare it with the standard Λ CDM model with $(\Omega_K, h, \omega_b, \omega_{cdm}, A_s, n_s, \tau_{reio})$ in the following manner. For suitable ranges of the parameters, the corresponding power spectra can be generated via CLASS, which can then be plotted to yield the corresponding curve. Each curve being the discrete power spectrum over the multipole moment parameter ℓ , its Euclidean distance to the Planck experimental curve can therefore be defined. By direct scan it is possible to determine the values of the cosmological parameter set that yields the minimum distance to the Planck 2018 curve. To provide assurance for the result, we also employ statistical and machine learning techniques. While the Planck analysis focused on observational data with advanced Bayesian methods, the present work employs statistical and machine learning regression techniques, specifically quartic regression, to compare the predictive accuracy and generalizability of the two models. Both 7- and 8 parameter models demonstrate exceptional accuracy, with the values of R^2

(coefficient of determination) nearing 99.9 % for training- as well as testing- dataset. This metric, with mean squared error (MSE), highlights the model’s ability to accurately capture the underlying variance of the distance variable while maintaining low error rates. The results are then compared to the CLASS default model (6 parameters) and the Planck 2018 model (7 parameters).

The rest of the paper is organized as follows. In section 2, we begin by recalling the key results from the work [7] on the finite-temperature quantum gravity (QG) effects. In section 2.1, we adopt Weinberg’s approach [1], essentially reproducing the power spectrum plot derived therein, and compare it with the Planck 2018 results [3]. Although Weinberg’s formalism is not suitable for a detailed comparison with current data, it serves as a useful starting point. This approach aids in understanding the underlying physics at intermediate steps and also provides an analytic expression for the final CMB power spectrum, $\frac{\ell(\ell+1)}{2\pi}C_\ell$. Following this, we examine the temperature-corrected cosmological constant (CC). Using Mathematica, we compute the values of the cosmological parameters, modified by the presence of the time-dependent CC, that best fit the fiducial Planck 2018 results. Many of the steps from Chapters 6 and 7 of [1] can be carried over with minimal modifications. For clarity, we demonstrate the analysis by including Ω_2 but omitting Ω_3 to keep the Mathematica calculations manageable in terms of memory usage. In section 3, we employ a quantum-modified version of the CLASS model [17], which includes the additional parameters Ω_{Λ_2} and Ω_{Λ_3} , and obtain the best fit for the 2018 Planck data [3]. Initially, we perform a brute-force parameter scan, revealing that the theoretical power spectrum is sensitive to both Ω_{Λ_2} and Ω_{Λ_3} , along with the other six parameters. Given the inherent randomness in the sampling method adopted, we validate these results using an independent method. Specifically, we apply various machine learning techniques to assess the predictive performance of both the 7-parameter and 8-parameter models in estimating the distance variable. By employing quartic regression, we optimize the feature values to minimize the predicted distance. The inclusion of Ω_{Λ_2} in the 8-parameter model proves to be valuable, as it improves the accuracy of the predictions while maintaining strong generalizability. Finally, in section 4, we conclude with a summary and potential directions for future research.

2 Finite-T effects on cosmological parameters

Finite-temperature one-loop renormalization analysis of the Standard Model coupled with gravity has been recently carried out [7]. The coupling constants, in particular, the cosmological constant, are shifted by temperature-dependent - thus time-dependent - quantum corrections. In this section, as a warm-up, we study the implications of the presence of Ω_{Λ_2} for $(h, \omega_b, \omega_{cdm}, A_s, n_s, \tau_{reio})$ by adopting and extending Weinberg’s semi-analytic formalism. The reason for employing the Weinberg’s formalism prior to a more precise numerical analysis by CLASS is that the former has the analytic final expression for the CMB power spectrum, $\frac{\ell(\ell+1)}{2\pi}C_\ell$. The Weinberg’s approach captures physics of the processes involved. By considering both approaches one can grasp intuition as well as accuracy.

2.1 Angular power spectrum in Weinberg's approach

We begin with a lightning review CMB angular power spectrum computation in [1]. There are two main components in the analysis therein: the fractional ionization X and the power spectrum itself $C_{TT,l}^S$ given in (2) and (8) below, respectively. The subscripts TT denote temperature-temperature correlation and S scalar. The fractional ionization X is defined as

$$X = \frac{n_e}{n}, \quad n = n_p + n_H. \quad (1)$$

where n_e, n_p, n_H denote the density of electrons, protons, hydrogens, respectively. It obeys

$$\frac{dX}{dT} = \frac{n\alpha}{TH} \left(1 + \frac{\tilde{\beta}}{\Gamma_{2s} + \frac{8\pi H}{\lambda_\alpha^3 n(1-X)}} \right)^{-1} \left(X^2 - \frac{1-X}{S} \right) \quad (2)$$

where

$$\begin{aligned} H &= 7.204 \times 10^{-19} T^{\frac{3}{2}} \sqrt{1.523 \times 10^{-5} T + h^2 \left(\frac{2.725}{T} \right)^3 \Omega_{\Lambda_1} + h^2 \Omega_M}, \\ \alpha &= \frac{1.4377 \times 10^{-10} T^{-0.6166}}{5.085 \times 10^{-3} T^{0.53} + 1} \text{ cm}^3 \text{ s}^{-1}, \quad \tilde{\beta} = 2.4147 \times 10^{15} \text{ cm}^{-3} e^{-39474/T} T^{\frac{3}{2}} \alpha, \\ \Gamma_{2s} &= 8.22458 \text{ s}^{-1}, \quad \lambda_\alpha = 1215.682 \times 10^{-8} \text{ cm}, \quad S = 1.747 \times 10^{-22} e^{157894/T} T^{\frac{3}{2}} \Omega_B h^2. \end{aligned} \quad (3)$$

The $h^2 \left(\frac{2.725}{T} \right)^3 \Omega_{\Lambda_1}$ term in H is small and can be disregarded [1]. We have used $\tilde{\beta}$, instead of β in [1], to avoid confusion with the integration variable β appearing in (8) below. This result is obtained with a commonly adopted assumption that the radiation is viewed to suddenly go from thermal equilibrium with matter to a free expansion at the red shift z_L . The quantitative definition of the corresponding temperature T_L is based on the so-called visibility function associated with the fractional ionization. To calculate T_L , consider the opacity

$$\mathcal{O} = 1 - \exp \left[- \int_{t(T)}^{t_0} c\sigma_T n_e dt \right] = 1 - \exp \left[- c\sigma_T \int_{T_0}^T dT' \frac{n_e(T')}{H(T')T'} \right] \quad (4)$$

where $\sigma_T = 0.66525 \times 10^{-24} \text{ cm}^2$, and the visibility function (it is usually defined in terms of $z, g(z)$.)

$$g(T) = \frac{d}{dT} \exp \left[- c\sigma_T \int_{T_0}^T dT' \frac{n_e(T')}{H(T')T'} \right] = \frac{d}{dT} \exp \left[- c\sigma_T \int_{T_0}^T dT' \frac{n(T')X(T')}{H(T')T'} \right] \quad (5)$$

where $n_e = nX$ was used in the second equality. The explicit form of n is

$$n = 0.76 \frac{3H_0^2 \Omega_B}{8\pi G m_p} \left(\frac{T}{T_{\gamma 0}} \right)^3 \quad (6)$$

The last scattering temperature T_L is defined by

$$\left. \frac{dg}{dT} \right|_{T=T_L} = 0. \quad (7)$$

As for $C_{TT,\ell}^S$, after extensive analysis it was shown in [1] that the power spectrum formula is given by:

$$\begin{aligned} \frac{l(l+1)}{2\pi} C_{TT,l}^S &= \frac{4\pi}{25} T_0^2 N^2 e^{-2\tau_{reion}} \int_1^\infty d\beta \left(\frac{\beta l}{l_{\mathcal{R}}} \right)^{n_S-1} \\ &\left\{ \frac{3(\beta^2-1)^{\frac{1}{2}}}{\beta^4(1+R_L)^{\frac{3}{2}}} e^{-2\beta^2 l^2/l_D^2} \mathcal{S}^2(\beta l/l_T) \sin^2\left(\beta l/l_H + \Delta(\beta l/l_T)\right) \right. \\ &\left. + \frac{1}{\beta^2(\beta^2-1)^{\frac{1}{2}}} \left[3\mathcal{T}(\beta l/l_T) R_L - (1+R_L)^{-\frac{1}{4}} e^{-\beta^2 l^2/l_D^2} \mathcal{S}(\beta l/l_T) \cos\left(\beta l/l_H + \Delta(\beta l/l_T)\right) \right]^2 \right\}. \end{aligned} \quad (8)$$

Above, N is a normalization paramter and τ_{reion} denotes the optical depth of reionized plasma. By following [1] we set

$$\frac{4\pi}{25} T_0^2 N^2 e^{-2\tau_{reion}} = 519.7 \mu K^2. \quad (9)$$

R_L is defined as the ratio of the background baryon and photon densities

$$R_L \equiv \frac{3}{4} \frac{\rho_B}{\rho_\gamma} \Big|_{z=z_L} = \frac{3\Omega_B}{4\Omega_\gamma} \frac{1}{(1+z_L)}. \quad (10)$$

The transfer functions $\mathcal{S}, \mathcal{T}, \Delta$ were numerically determined and given by

$$\begin{aligned} \mathcal{S}(\kappa) &\equiv \left(\frac{5^{1/2}(0.1657\kappa)^6 + (0.5116\kappa)^4 + (1.209\kappa)^2 + 1}{(0.1657\kappa)^6 + (0.4249\kappa)^4 + (0.9459\kappa)^2 + 1} \right)^2 \\ \mathcal{T}(\kappa) &\equiv \frac{\log[(0.124\kappa)^2 + 1]}{(0.124\kappa)^2} \sqrt{\frac{(0.2197\kappa)^6 + (0.4452\kappa)^4 + (1.257\kappa)^2 + 1}{(0.3927\kappa)^6 + (0.8568\kappa)^4 + (1.606\kappa)^2 + 1}} \\ \Delta(\kappa) &\equiv \left(\frac{(0.2578\kappa)^6 + (0.5986\kappa)^4 + (1.1547\kappa)^2}{(0.2204\kappa)^8 + (0.4581\kappa)^6 + (0.8707\kappa)^4 + (1.723\kappa)^2 + 1} \right)^{\frac{1}{4}}. \end{aligned} \quad (11)$$

The definitions of $l_T, l_D, l_H, l_{\mathcal{R}}$ are as follows:

$$l_T \equiv \frac{d_A}{d_T}, \quad l_D \equiv \frac{d_A}{d_D}, \quad l_H \equiv \frac{d_A}{d_H}, \quad l_{\mathcal{R}} \equiv (1+z_L) k_{\mathcal{R}} d_A \quad (12)$$

where the arbitrary pivot scale $k_{\mathcal{R}}$ is chose to be = 0.05, and d_T , the acoustic horizon distance at last scattering d_H , and the angular diameter distance d_A are given by

$$\begin{aligned} d_T &\equiv \kappa \frac{a_L}{q} = \frac{\sqrt{\Omega_R}}{(1+z_L) H_0 \Omega_M} \\ d_H &\equiv \frac{2}{H_0 \sqrt{3R_L \Omega_M} (1+z_L)^{3/2}} \ln \left(\frac{\sqrt{1+R_L} + \sqrt{R_{EQ} + R_L}}{1 + \sqrt{R_{EQ}}} \right) \\ d_A &\equiv r_L a_L = \frac{1}{H_0} \frac{1}{1+z_L} \int_{(1+z_L)^{-1}}^1 \frac{dx}{\sqrt{\Omega_\Lambda x^4 + \Omega_M x}} \end{aligned} \quad (13)$$

respectively. The symbols κ, R_{EQ} are defined as

$$\kappa \equiv \frac{\sqrt{2} q}{a_{EQ} H_{EQ}}, \quad R_{EQ} = \frac{3 \rho_B}{4 \rho_\gamma} \Big|_{z=z_{EQ}}. \quad (14)$$

For damping distances one has,

$$d_D^2 = d_{\text{Landau}}^2 + d_{\text{Silk}}^2 \quad (15)$$

where, for Landau damping,

$$d_{\text{Landau}}^2 = \frac{3\sigma^2 t_L^2}{8T_L^2(1+R_L)} \quad (16)$$

where σ denotes the standard deviation of $\mathcal{O}'(T)$ when approximated as a Gaussian distribution, and

$$d_{\text{Silk}}^2 = \frac{cR_L^2}{6(1-Y)n_{B0}\sigma_\tau H_0 \sqrt{\Omega_B} R_0^{9/2}} \int_0^{R_L} \frac{R^2 dR}{X(1+R)\sqrt{R_{EQ}+R}} \left(\frac{16}{15} + \frac{R^2}{1+R} \right) \quad (17)$$

for Silk damping. The parameter t_L in the Landau damping can be computed by the general formula for the time for an event with the red shift z

$$t(z) = \frac{1}{H_0} \int_0^{\frac{1}{1+z}} \frac{dx}{x} \left[\Omega_\Lambda + \Omega_M x^{-3} + \Omega_R x^{-4} \right]^{-\frac{1}{2}}. \quad (18)$$

Before delving into the finite-temperature corrections in the next section, we would like to briefly comment on some of the approximations made in the analysis of [1]. In addition to the approximation of treating recombination as nearly instantaneous, several other approximations and simplifications were made. For example, the integrated Sachs–Wolfe effect, which primarily affects small values of ℓ , was neglected. Additionally, the tight coupling approximation was used for the early photon-baryon fluid. (The CLASS model, in contrast, accounts for these effects with greater accuracy.) Furthermore, although less significant, there are minor "discrepancies" between the results obtained by Weinberg and those presented in the present work. For instance, consider the last two rows in Table 2.3 of [1]. When using the same data from that table, the values for the standard deviations turned out to be slightly different in our analysis. This indicates that there is a small program-dependence in the computation of sigma.

2.2 Finite-temperature modifications

Finite-temperature effects feed the CC through perturbative loops. The CC thus becomes temperature-dependent for a FLRW background. The resulting CC can be viewed as a form of early dark energy that has been present and significant up until around matter-radiation equality. One might mistakenly assume that finite-temperature quantum loop-induced contributions to the cosmological constant, such as those involving photons and neutrinos, are already included as part of the radiation contribution. However, this view overlooks the role

of virtual particles in the cosmological constant. The contributions from Standard Model particles (and gravitons) arise from the vacuum energy of virtual particles, while radiation corresponds to the energy density of physical, onshell particles moving through the Universe.

As mentioned earlier, the crux of our approach lies in the introduction of Ω_{Λ_2} (and Ω_{Λ_3}). The analysis in section 3 shows that Ω_{Λ_2} is on the order of 10^{-8} . We view these parameters as phenomenological. However, in section 3.3, we will discuss the (un)naturalness of the order of Ω_{Λ_2} , specifically its value of 10^{-8} , by introducing a different renormalization scheme that is better suited for this purpose.

For the analysis in section 3.3, we bring home the distinction between the zero-temperature contributions and the finite-temperature contributions. For the CC problem, the role of the temperature dependence terms was more highlighted [5], [6]. This difference is due to the slight change of the renormalization schemes. Let us recall the renormalization of the cosmological constant proposed in [5] [6], and [7]. It was demonstrated that the one-loop correction is two or three orders of magnitude smaller than the observed value. The essential idea can be explained by considering a gravity-scalar system

$$S = \frac{1}{\kappa^2} \int d^4x \sqrt{-g} R - \int d^4x \sqrt{-g} \left(\frac{1}{2} g^{\mu\nu} \partial_\mu \zeta \partial_\nu \zeta + V(\zeta) \right) \quad (19)$$

where $\kappa^2 = 16\pi G$ with G being Newton's constant. The potential $V(\zeta)$ is

$$V(\zeta) = \frac{\lambda}{4!} \left(\zeta^2 + \frac{6}{\lambda} \nu^2 \right)^2. \quad (20)$$

The cosmological constant (CC) value depends, of course, on whether one adopts the complete-square form or the version without the constant term. (Whether to use the complete-square form or the traditional one is not central to the CC problem.) For the onshell potential value, one gets [5] [6]

$$V = -\frac{1}{90} \pi^2 T^4 + \dots \quad (21)$$

where the ellipsis includes terms that depend on the mass of the scalar. Let us choose the renormalized mass value appropriately to deal with the CC problem: set the renormalized mass of the scalar particle so that it is on the order of the temperature. At the same time let it be sufficiently smaller than the temperature so that their contributions to the CC can be disregarded. With this renormalization scheme, the leading term in the potential is $\sim T^4$, as indicated above. Evaluated at the present temperature of the Universe, this implies that there is a order 10^{4-5} gap between the value above and the observed value of the CC, a (potentially) big improvement from the gap noted in the CC problem. As anticipated in [5], once one considers the Standard Model (SM), its particle content should further reduce the gap. To see this, note that a fermionic field contributes

$$\frac{7}{8} \frac{\pi^2}{90} T^4 + \dots \quad (22)$$

to the potential. By going over the contributions of the SM particles, which provides an additional factor of around 120, the CC order discrepancy is now reduced from 10^{60} to

10^{2-3} .³ This observation was based on the one-loop correction, which has been shown to be two or three orders of magnitude smaller than the observed value, as just stated. However, it is possible to introduce a classical contribution to the cosmological constant (CC), and it is standard practice in renormalization to include such a classical term, the renormalized CC, Λ_{ren} , with the corresponding expression added to the density parameter. With this approach, the unnaturalness of adding or subtracting extremely large and small numbers is no longer present [5–7]. (This approach, however, comes with a trade-off, as reviewed in Section 3.3.)

With the role of the leading T -dependent part of the vacuum energy in dealing with the CC problem understood, one can consider the finite- T contributions for the present purpose. (Here we are implicitly employing a new renormalization scheme more convenient for the task at hand; see section 3.3. As we will discuss below in more detail, the motivation for this is to avoid the unnaturalness of the order of Ω_{Λ_2} , 10^{-8} .) Let us now consider conducting cosmological perturbation analysis with the 1PI action (with only the first few leading-order terms kept) coupled with the hydrodynamic (or Boltzmann) system. One of the implications of [5–7] is that the leading quantum corrections yield the following form of the time-dependent vacuum energy⁴

$$\Lambda(t) = \Lambda_1 + \Lambda_2 \left(\frac{a_0}{a}\right)^4 + \Lambda_3 \left(\frac{a_0}{a}\right)^2 + \dots \quad (23)$$

where Λ_1, Λ_2 are time-independent constants, with $\Lambda_1 + \Lambda_2 + \Lambda_3 + \dots$ representing the known present value of the CC. The time-dependent CC in eq. (23) introduces additional density parameters, Ω_{Λ_2} and Ω_{Λ_3} , corresponding to the a^{-4} - and a^{-2} -scalings, respectively, in addition to the usual density parameter Ω_{Λ_1} . Although the CC term associated with Ω_{Λ_2} scales as $1/a^4$, it does not correspond to radiation, since radiation must satisfy $p = \rho/3$. Similarly, Ω_{Λ_3} , which appears in the off-shell action through quantum corrections, is conceptually distinct from Ω_K , which is associated with the parameter K in the on-shell solution.⁵

For Mathematica analysis we only include Ω_2 , but not Ω_3 , to keep the analysis manageable. The parameter Ω_3 will be included in section 3 where the analysis by employing CLASS is carried out. The presence of an additional density parameter, Ω_{Λ_2} , manifests itself only through the Hubble parameter H . Let us enumerate the channels through which the addi-

³The details of renormalization analysis can be quite subtle. For the zero- T component, the bosonic and fermionic contributions tend to cancel each other out due to their opposite signs. However, for the T^4 term, the situation is different: the one-loop bosonic and fermionic contributions carry a negative sign, so the fermionic contributions add to the bosonic ones. Given that there are more fermionic degrees of freedom than bosonic ones in the SM (coupled with gravity), the relative magnitudes of these contributions must be carefully balanced by adjusting the renormalized masses of the bosonic and fermionic fields to ensure the correct sign for the overall cosmological constant (CC). This balancing act can be helped by adjusting, if necessary, the finite parts of the renormalization parameters, often denoted as c 's in renormalization theory. These c 's play a crucial role in the proposed resolution of the CC problem.

⁴Since higher-order loop corrections are among the terms represented by (\dots) , additional time-dependent terms with different a -scalings will arise. These terms are not considered in the present work, although they will be addressed in the conclusion.

⁵At the technical level of the perturbation analysis, however, these two cannot be distinguished. In the analysis presented in section 3, we let Ω_{Λ_3} to take on the role of Ω_K , setting the latter to zero in the modified CLASS system.

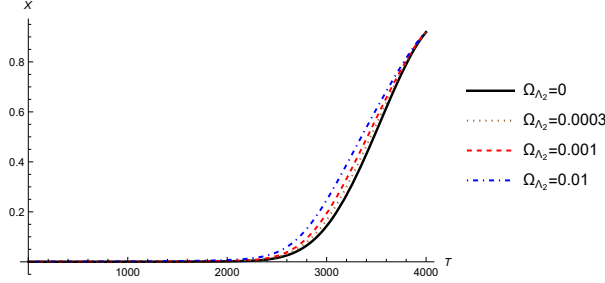


Figure 1: typical behaviors of the fractional ionization X as a function of Ω_{Λ_2} ; four arbitrary values of Ω_{Λ_2} are chosen for demonstration

tional density parameter, Ω_{Λ_2} , modifies various cosmological parameters. First, the presence of Ω_{Λ_2} modifies the fractional ionization X through the modified H ,

$$H = 7.204 \times 10^{-19} T^{\frac{3}{2}} \sqrt{1.523 \times 10^{-5} T + \left(\frac{2.725}{T}\right)^3 \Omega_{\Lambda_1} h^2 + \Omega_M h^2 + \frac{T}{2.725} \Omega_{\Lambda_2} h^2}. \quad (24)$$

The modification of X leads, via eq. (7), to a modified value of z_L , thus other quantities, such as R_L , as well. The power spectrum formula eq. (8) was obtained by first obtaining a semi-analytic solution - the analysis carried out in Ch. 6 of [1] - and substituting it into a two-point correlator of the temperature variation. The analysis of Ch. 6 of [1] can be carried over with the minor change of H , eq. (24), whenever it appears. As for $C_{TT,l}^S$ in eq. (8), one can use $\mathcal{T}, \mathcal{S}, \Delta$ without modifications. The finite-T corrections modifies d_A and $d_D, d_T, d_H, l_{\mathcal{R}}$ as well through the modification of the former:

$$d_A = \frac{2.9979 \times 10^3}{(1 + z_L) \sqrt{\Omega_{\Lambda_1} h^2 x^4 + \Omega_M h^2 x + (\Omega_{\Lambda_2} + \Omega_R) h^2}}. \quad (25)$$

Fig. 1 shows sample plots of X for different values of Ω_{Λ_2} . Although X decreases slower toward lower temperature with increased values of Ω_{Λ_2} , explicit analysis based on eq. (7) reveals that the finite-T effect actually increase the value of T_L .

To obtain the CMB power spectrum in terms of the 7 parameters - six usual ones,

$$h, \Omega_B, \Omega_M, N, n_s, \tau_{reio}, \quad (26)$$

plus Ω_{Λ_2} , one should first obtain various parameters appearing the angular power spectrum in eq. (8), such as $l_T, l_D, l_H, l_{\mathcal{R}}$, as functions of the seven parameters. To keep the Mathematica numerical study manageable, for N, τ_{reio} , we adopt the values given in [1], and hone in on the dependence of the various parameters on four cosmological parameters, $(h, \Omega_B, \Omega_M, \Omega_{\Lambda_2})$. Determination of optimal n_s can be easily done at the final stage. In other words one can worry about n_s at the stage of evaluating $C_{TT,l}^S$ after determining $l_T, l_D, l_H, l_{\mathcal{R}}$ as functions of the independent cosmological parameters: most of our effort is made to obtain the dependences of $l_T, l_D, l_H, l_{\mathcal{R}}$ on the four parameters $(h, \Omega_B, \Omega_M, \Omega_{\Lambda_2})$. The expressions for $l_T, l_D, l_H, l_{\mathcal{R}}$ themselves contain parameters, such as $z_L, \sigma, R_L, R_{EQ}, t_L$ (where σ denotes the standard deviation of $\mathcal{O}'(T)$ when approximated as a Gaussian distribution), that need

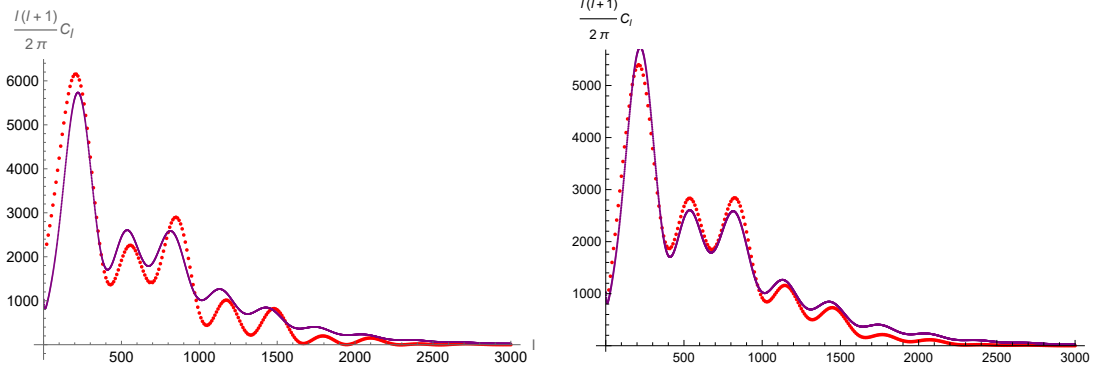


Figure 2: (a) $(h, \Omega_B, \Omega_{\Lambda_2})$ -interpolation (b) $(h, \Omega_M, \Omega_{\Lambda_2})$ -interpolation; for (a) $\Omega_M = 0.13299/h^2$. The best fit parameters are $(h, \Omega_B, \Omega_{\Lambda_2}, n_s) = (0.765515, 0.057172, 0.00005, 0.985064)$; for (b), $\Omega_B = 0.02238/h^2$. The best fit parameters are $(h, \Omega_M, \Omega_{\Lambda_2}, n_s) = (0.649838, 0.272761, -1.59513 \times 10^{-6}, 0.99)$

to be expressed in terms of the four parameters $(h, \Omega_B, \Omega_M, \Omega_{\Lambda_2})$ in order to quantitatively determine the values of the four parameters for the best fit. Although it would be ideal to obtain these parameters in terms of the full set, $(h, \Omega_B, \Omega_M, \Omega_{\Lambda_2})$, it again turns out that this is a highly memory-demanding procedure and requires more powerful computing resources (this was the case, for instance, for σ); we will not pursue this full task in the present work. Instead we group $(h, \Omega_B, \Omega_M, \Omega_{\Lambda_2})$ into $(h, \Omega_B, \Omega_{\Lambda_2})$ and $(h, \Omega_M, \Omega_{\Lambda_2})$, and separately study the dependence of the various parameters on each of these two groups. For each set of $(h, \Omega_M, \Omega_{\Lambda_2})$ and $(h, \Omega_B, \Omega_{\Lambda_2})$, the power spectrum is obtained. Two examples of the plots are given in Fig. 2.⁶

To obtain the CMB power spectrum in terms of the seven parameters—six usual ones,

$$h, \Omega_B, \Omega_M, N, n_s, \tau_{\text{reio}}, \quad (27)$$

plus Ω_{Λ_2} —one must first derive the various parameters that appear in the angular power spectrum in eq. 8, such as $l_T, l_D, l_H, l_{\mathcal{R}}$, as functions of the seven parameters. To keep the Mathematica numerical study manageable, we adopt the values of N and τ_{reio} from [1] and focus on how the parameters depend on four cosmological parameters, $(h, \Omega_B, \Omega_M, \Omega_{\Lambda_2})$. The determination of the optimal n_s can be done at the final stage. In other words, n_s can be addressed after evaluating $C_{TT,l}^S$, once the dependencies of $l_T, l_D, l_H, l_{\mathcal{R}}$ on the independent cosmological parameters are determined. Our main effort focuses on determining the dependencies of $l_T, l_D, l_H, l_{\mathcal{R}}$ on the four parameters $(h, \Omega_B, \Omega_M, \Omega_{\Lambda_2})$.

The expressions for $l_T, l_D, l_H, l_{\mathcal{R}}$ themselves involve parameters such as $z_L, \sigma, R_L, R_{EQ}, t_L$ (where σ denotes the standard deviation of $\mathcal{O}'(T)$, where \mathcal{O} is given in eq. (4), when approximated as a Gaussian distribution). These parameters need to be expressed in terms of $(h, \Omega_B, \Omega_M, \Omega_{\Lambda_2})$ in order to quantitatively determine the values of the four parameters for the best fit.

⁶A minor technical note is that the plot of the solid line is that based on CLASS default.ini file but not that of the Planck 2018 data. As we will see in the next section the two are visually indistinguishable. We happen to use the CLASS data since the range of ℓ is larger whereas that of Planck 2018 goes up to $\ell = 2508$.

Although it would be ideal to express these parameters in terms of the full set $(h, \Omega_B, \Omega_M, \Omega_{\Lambda_2})$, this turns out to be a highly memory-intensive process that requires more powerful computational resources (as was the case for σ , for instance). We will not pursue this full task in the present work. Instead, we group the parameters into two sets: $(h, \Omega_B, \Omega_{\Lambda_2})$ and $(h, \Omega_M, \Omega_{\Lambda_2})$, and separately study the dependence of the various parameters on each of these two groups. For each set, $(h, \Omega_M, \Omega_{\Lambda_2})$ and $(h, \Omega_B, \Omega_{\Lambda_2})$, we compute the power spectrum. Two examples of the resulting plots are shown in Fig. 2.⁷

3 Modified CLASS and machine learning techniques

Weinberg’s approach is insightful and valuable for understanding the physics of key events during the intermediate period between the generation of the CMB and its observation today. However, as noted in his book, its primary aim is not the precise calculation of the power spectrum curve. For such purposes, computational tools like CAMB or CLASS are typically employed. In this section, we utilize a finite-temperature modified version of CLASS and perform two types of analyses. The first analysis involves a brute-force scan, as described below. The second analysis complements the first by incorporating statistical and machine-learning techniques.

In the modified version of CLASS [17], the original Hubble constant $H(t)$ is replaced by the following that contains the finite-T corrections:

$$H = 7.204 \times 10^{-19} T^{\frac{3}{2}} \sqrt{1.523 \times 10^{-5} T + \left(\frac{2.725}{T}\right)^3 \Omega_{\Lambda_1} h^2 + \Omega_M h^2 + \frac{T}{2.725} \Omega_{\Lambda_2} h^2 + \frac{2.725}{T} \Omega_{\Lambda_3} h^2}. \quad (28)$$

Once the values of the cosmological parameters are fixed, the power spectra are computed using the modified CLASS. A large number of parameter sets can be scanned by running the CLASS Python wrapper, CLASSy. Each resulting spectrum is then fed into a code that calculates the Euclidean distance between the generated curve and the Planck data [3]. By these comprehensive scans and distance calculations we obtain tens of millions of data points. The details of the brute-force scan will vary slightly each time because the data collection procedure involves random sampling. It will be nice to check the qualitative features of the results by an independent method. For this purpose we employ machine learning techniques and evaluate the predictive performance of the models in estimating the distance.

We consider two cosmological models: the first is the original Λ CDM model, which has 7 parameters: $(\Omega_K, h, \omega_b, \omega_{cdm}, A_s, n_s, \tau_{\text{reio}})$. The second model incorporates finite-T QG effects and has 8 parameters: $(\Omega_{\Lambda_2}, \Omega_{\Lambda_3}, h, \omega_b, \omega_{cdm}, A_s, n_s, \tau_{\text{reio}})$. For each model, we use 5000 datasets, selected from a much larger data sample as explained below. We then apply a regression-based machine learning technique to estimate the minimum distance between the generated spectra and the Planck 2018 data.

⁷A minor technical note: the solid line in the plot is based on the CLASS default.ini file, not the Planck 2018 data. As we will see in the next section, the two are visually indistinguishable. We used the CLASS data because its ℓ -range is larger, while the Planck 2018 data extends only up to $\ell = 2508$.

The objective is to determine which model best explains the variance in the target variable, the distance d , while balancing model complexity and performance. Model selection is based on maximizing R^2 and minimizing the MSE in both training and testing datasets. Using quartic regression, which proves to be the best-performing model, we compare the accuracies and generalization capabilities of both models. The comparison shows that including the additional parameters from finite-temperature QG effects modifies the values of the cosmological parameters, resulting in an improved distance fit to the Planck 2018 data.

3.1 Brute-force scan by CLASSy

In the analysis by employing CLASS, we first conduct brute-force scans to systematically explore the parameter space for cosmological models. By generating discrete power spectra over the multipole moment parameter ℓ for suitable ranges of the parameters, their distances from the Planck 2018 experimental curve can be calculated. This approach requires extensive scanning of the parameter space, ultimately determining the set of cosmological parameters that minimizes the distance to the Planck 2018 curve. The brute-force method demands high-performance computing resources. Using CLASS, specifically its Python wrapper CLASSy, we conduct extensive parameter scans, ultimately collecting several tens of millions of datasets. This immense volume of data is necessary to perform various checks and validate the robustness of the results. Based on these preliminary explorations, appropriate parameter ranges are carefully refined. From these final intervals, we collect 400,000 datasets for the 7-parameter case and 300,000 datasets for the 8-parameter case. The number of the datasets for the 8-parameter model was deliberately chosen less than that of the 7-parameter model. This was to bring out the fact that the former performs better in spite of this disadvantage. See the related comments below. These tasks test the limits of our high-end personal computers, which, while capable, are pushed to their full capacity. (Despite leveraging a supercomputer for part of the data collection, the additional computational power offered minimal speed advantages, emphasizing the intense demands of such exhaustive analyses. See the conclusion for more.)

The impact of inclusion of Ω_{Λ_2} is reflected on the actual minimum values of the distance and the corresponding parameters set. For the 7-parameter model, the minimum distance of the 400,000 datasets is

$$d = 28.122388 \tag{29}$$

which occurs at

Ω_K	h	ω_b	ω_{cdm}	A_s	n_s	τ_{reio}
0.002339	0.677333	0.022387	0.119889	2.098889×10^{-9}	0.9660	0.054000

whereas for the 8-parameter model, the minimum of the 300,000 datasets is

$$d = 26.832229 \tag{30}$$

with

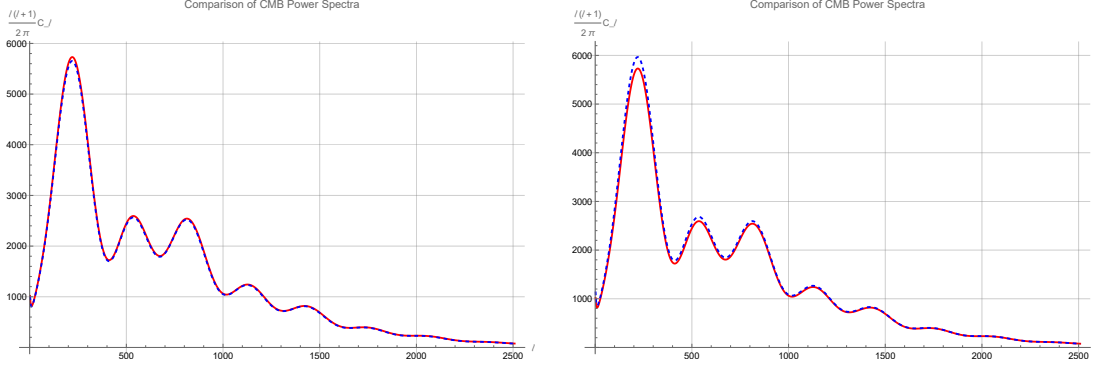


Figure 3: The dotted plot in panel (a) represents a curve with a distance $d \approx 1200$ from the Planck 2018 data, while the dotted plot in panel (b) corresponds to a distance $d \approx 3400$.

Ω_{Λ_2}	Ω_{Λ_3}	h	ω_b	ω_{cdm}	A_s	n_s	τ_{reio}
-2.073444×10^{-8}	0.004297	0.675500	0.022394	0.119889	2.101111×10^{-9}	0.966000	0.054444

Note that these minima are actual data values. Below we obtain the regression functions of these two datasets and obtain the minima (given in the "Range" columns of the table in Fig. 4) predicted by the functions. Those minima will in turn be checked against the values (given in (31)) yielded by directly running CLASS with the corresponding values of the parameters as input. To provide some context for the distance values, we show two plots in Fig. 3. As seen in these plots, the curves with distances in the range of several hundreds are nearly identical to the Planck 2018 curve, appearing directly on top of it.

The analysis of the 8-parameter model, based on 300,000 datasets, compared to the 400,000 datasets used for the 7-parameter model, highlights an inherent limitation in the dataset sizes and their comparability. Given that the 8-parameter model includes one additional parameter, a fair comparison would require a dataset larger than 400,000 by some appropriate factor to adequately cover the expanded parameter space. Despite this discrepancy, the results indicate that the minimum distance to the Planck 2018 curve is smaller for the 8-parameter model, an important feature shared by the statistical analysis below. Its inclusion clearly enhances the model's ability to align more closely with the data, reinforcing the critical role of Ω_{Λ_2} in achieving the optimal curve.

3.2 Analysis by statistical and machine learning techniques

Involving random sampling, the specifics of the brute-force scan may vary slightly with each iteration. It would be reassuring to access the qualitative aspects of the results using an independent method. For this, we apply statistical and machine learning techniques to evaluate the predictive performance of the two cosmological models in estimating the distance variable. The minimum distance predicted by each model is explicitly checked by running CLASS with the corresponding set of the cosmological parameters; see eq. (31) below. Here are some details of the analysis.

The dataset comprises 5,000 observations, i.e., sets of the parameters, for both the 7-parameter and 8-parameter models. To ensure sufficient data for model validation using

10-fold cross-validation, with each fold containing at least 500 samples, the 5,000 minimum-distance data samples are selected from a total of 400,000 and 300,000 CLASSy-generated datasets for the 7-parameter and 8-parameter models, respectively. Each dataset is then split into a training set (70%), consisting of 3,500 datasets, and a testing set (30%), consisting of 1,500 datasets. To address differences in the scales of independent parameters, all features are standardized, which transforms each variable to have a mean of 0 and a standard deviation of 1. This mitigates bias toward features with larger ranges and ensures uniform contribution of all variables to the regression analysis.

The performance of the polynomial regression models is evaluated using R^2 , which quantifies the proportion of variance in the dependent variable modeled by the independent variables. Additionally, the MSE used to measure the average squared difference between predicted and actual values, providing a complementary metric to evaluate model performance. Both models achieve exceptional accuracy, with the R^2 values nearing 99.9%. The inclusion of Ω_{Λ_2} in the 8-parameter model introduces additional complexity, which increases the data requirements for achieving stabilization on the learning curve. However, this added complexity ultimately enhances the model’s predictive accuracy. The table in Fig. 4 presents a detailed statistical summary of the key variables in the 7-parameter and 8-parameter models. Notably, the addition of Ω_{Λ_2} in the 8-parameter model introduces subtle shifts in other variables, such as h , n_s , and τ_{reio} . These shifts are accompanied by slightly increased variability in the distance value, as reflected in its higher standard deviation and wider range in the 8-parameter model compared to the 7-parameter model. A series of regression models, ranging from linear regression to polynomial regression up to degree 10, are evaluated for both datasets. The models are built and assessed separately for the 7-parameter and 8-parameter datasets. The quartic regression model (polynomial degree = 4) emerged as the best-performing one based on R^2 and MSE, as it consistently explains the largest proportion of variance in both the training and testing datasets, compared with higher-degree polynomials that exhibit overfitting tendencies.

The R^2 metric is calculated separately for the training and testing datasets to evaluate the models’ ability to generalize. For the 7-parameter model, the quartic regression achieves an R^2 of 99.90% on the training set and 99.88% on the testing set, with MSE values of 0.0713 and 0.0795, respectively. In the 8-variable model, including Ω_{Λ_2} improved the training R^2 to 99.92%, though the testing R^2 remained at 99.88%, with MSE values of 0.0792 and 0.1096. While the addition of Ω_{Λ_2} slightly increases the error on the testing set, overall performance remained strong. Figs. 5 and 6 visually confirm these results, showing the predicted versus actual values and residual distributions for both models. The plots reveal a near-perfect alignment along the diagonal.

The learning curves for the 7-parameter and 8-parameter models, shown in Figs. 8 and 9, provide valuable insights into how training and validation accuracy evolve as the number of training samples increases. Both models ultimately achieve high accuracy, with training and validation accuracies converging near 99%, highlighting the effectiveness of the quadratic regression approach in predicting the distance variable. For the 7-parameter model, stability is reached around 1,000 training samples, where both accuracies consistently approach 99%. In contrast, the 8-parameter model, which includes the additional parameter Ω_{Λ_2} , requires a significantly larger dataset to stabilize. Stability is achieved at approximately 2,500 training

Variable	Count	$(\Omega_K, 6 \text{ variables})$ model			$(\Omega_{\Lambda 2}, \Omega_{\Lambda 3}, 6 \text{ variables})$ model		
		Mean	STD	Range	Mean	STD	Range
Distance	5000	55.75	8.19	[28.12, 66.92]	58.80	9.70	[26.83, 71.76]
$\Omega_{\Lambda 3}$					-2.07E-08	2.32E-11	[-2.075E-08, -2.068E-08]
$\Omega_{\Lambda 2}$	5000	0.002336	0.000003	[0.00233, 0.002342]	0.004289	0.00002	[0.00425, 0.00431]
h	5000	0.676876	0.000624	[0.676, 0.678]	0.675491	0.000325	[0.675, 0.676]
ω_b	5000	0.022376	0.000027	[0.02232, 0.02242]	0.022393	0.000028	[0.02235, 0.02245]
ω_{cdm}	5000	0.119924	0.000207	[0.11944, 0.12033]	0.119853	0.00018	[0.11944, 0.12033]
A_s	5000	2.10E-09	3.58E-12	[2.09E-09, 2.1056E-09]	2.10E-09	2.98E-12	[2.0967E-09, 2.1100E-09]
n_s	5000	0.965761	0.000491	[0.965, 0.967]	0.965896	0.000487	[0.965, 0.967]
τ_{reio}	5000	0.053948	0.000757	[0.052, 0.055]	0.054819	0.000595	[0.054, 0.056]

Figure 4: Statistical summary of variables in the 7-parameter and 8-parameter models

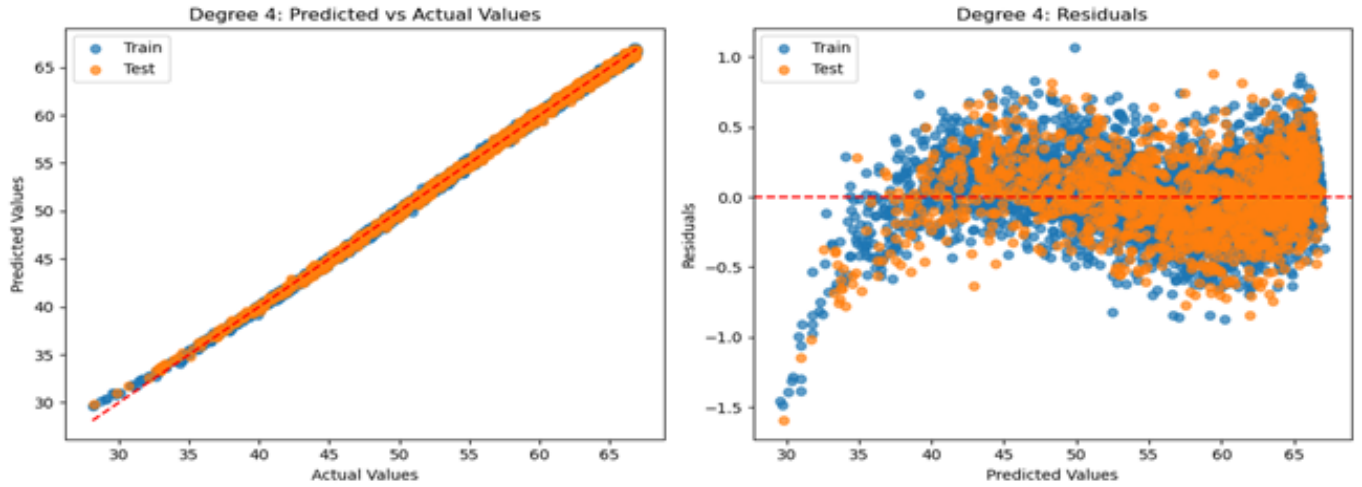


Figure 5: 7-parameter model estimation and residuals

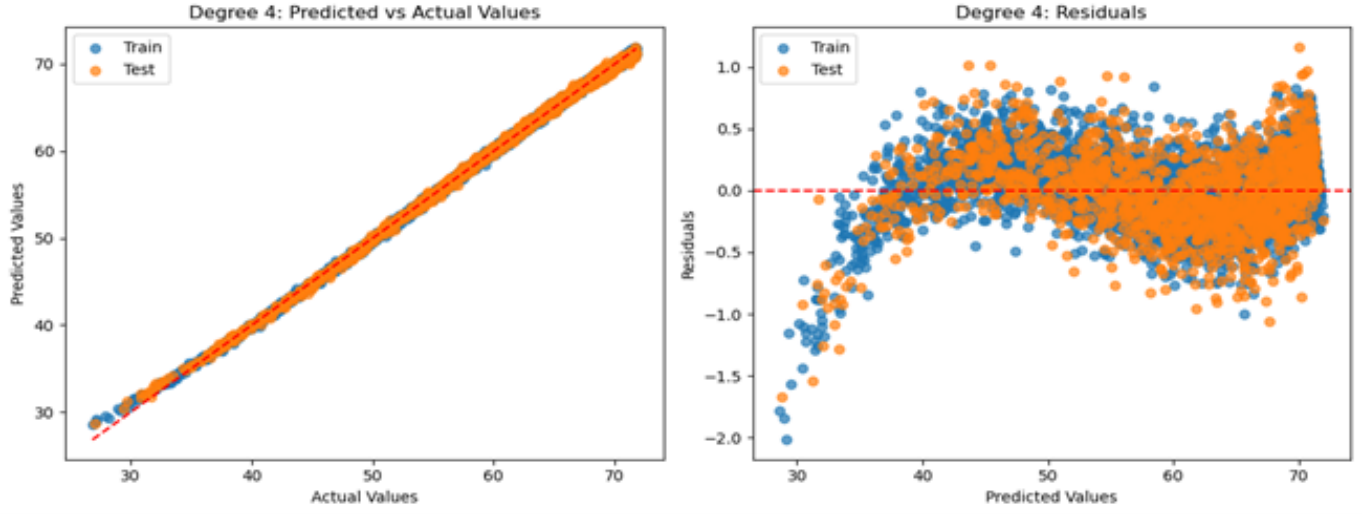


Figure 6: 8-parameter model estimation and residuals

Variable	7-parameter Model	8-parameter Model
$\Omega_{\Lambda 2}$	-	-2.08E-08
$\Omega_K/\Omega_{\Lambda 3}$	0.00233471	0.00432285
h	0.67733813	0.67536996
ω_b	0.02238564	0.02238631
ω_{cdm}	0.11984093	0.11985634
A_s	2.09E-09	2.09E-09
n_s	0.96599393	0.96583361
τ_{reio}	0.05295666	0.0530449
Predicted distance	27.877821	24.391195

Figure 7: Optimized feature values for minimum distance in 7- and 8- parameter models

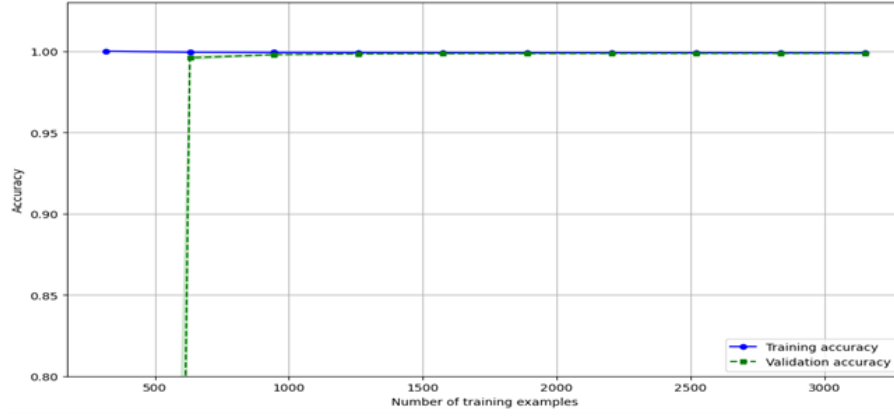


Figure 8: Learning curve of 7 parameter model

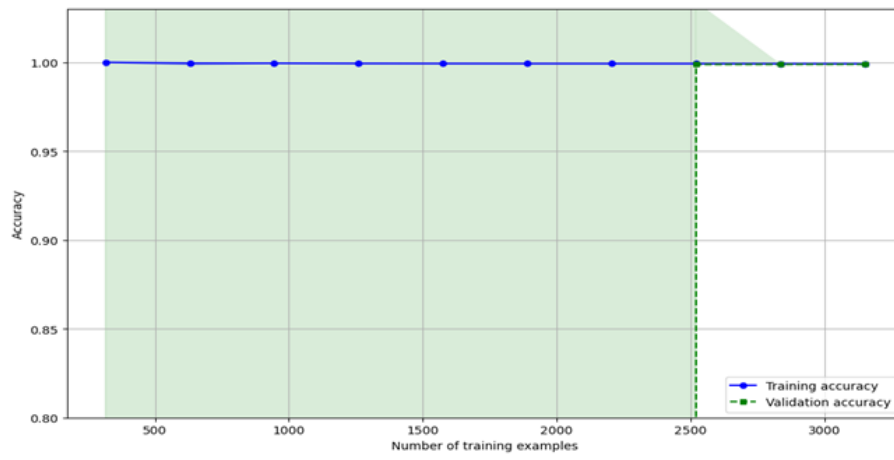


Figure 9: Learning curve of 8-parameter model

samples, with both accuracies converging near 99%. This extended stabilization period reflects the added complexity introduced by the extra parameter, which necessitates a larger dataset for effective generalization. Despite the inclusion of Ω_{Λ_2} , key parameters such as A_s and ω_b remain highly stable across both models, demonstrating their robustness to changes in model complexity. The wider range and increased variability in the 8-parameter model underscore its ability to capture more aspects of cosmological phenomena while maintaining the reliability of the core parameters.

Minimum distance prediction and check

The regression results show that the 7-parameter and 8-parameter models predict minimum distance values of 27.88 and 24.39 (rounded), respectively; see the table in Fig. 7. While the 8-parameter model achieves a lower predicted minimum distance, the inclusion of Ω_{Λ_2} in the 8-parameter model led to adjustments in other feature values, most notably Ω_{Λ_3} , which influenced the predicted distance outcome. To validate these predictions, we calculated the distances for the corresponding parameters values; the actual CLASS-computed distance values turn out to be

distance of 7-parameter model	distance of 8-parameter model	(31)
26.03	24.95	

where the values have been rounded. This result demonstrates a close alignment with the polynomial regression model’s predictions, and confirms that the 8-parameter model achieves a slightly lower minimum distance.

3.3 (Un)naturalness of the order of Ω_{Λ_2}

Let us now consider the naturalness of the order of magnitude of Ω_{Λ_2} , which has been found to be on the order of 10^{-8} . The solution to the CC problem proposed in [5–7], which was briefly reviewed in section 2, suggests that Ω_{Λ_2} should be related to Ω_{Λ_1} through a factor of $10^{-(2\sim 3)}$, i.e., $\Omega_{\Lambda_2} \sim \Omega_{\Lambda_1} \times 10^{-(2\sim 3)}$. Given that $\Omega_{\Lambda_1} \simeq 0.7$, the natural expectation for the order of Ω_{Λ_2} is $\Omega_{\Lambda_2} \simeq 10^{-(3\sim 4)}$. However, the numerical analysis carried out in the present study yields a value of $\Omega_{\Lambda_2} \sim 10^{-8}$, which is several orders of magnitude smaller than the expected range of $10^{-(3\sim 4)}$.

This discrepancy, where the order of 10^{-8} seems much smaller than the expected $10^{-(3\sim 4)}$, raises the question of whether this result is unnatural, and if so, whether it can be explained. It would indeed be beneficial to explore this gap further and attempt to provide at least some level of explanation for it. However, before delving into a more detailed analysis, let us briefly recall the nature of the proposal in [5–7] and the challenges it presents.

The solution of the CC problem suggested in [5–7] is not without its “cost.” This cost, however, is not unique to the proposal at hand, but rather reflects a more general phenomenon inherent in renormalization schemes. The approach used in those works involves an appropriate renormalization scheme, and as such, it is not free from a certain degree of unnaturalness when applied to other problems. As well known, physical quantities must be independent of the renormalization schemes used. There are infinitely many renormalization schemes that differ by finite renormalization. It is possible, and often necessary, to

change the renormalization scheme when an initial choice made for one problem becomes inconvenient for another.

In the case of the CC problem, this unnaturalness, which is nothing but the well-known fine-tuning, arises specifically due to the onshell renormalization scheme. This scheme uses the physical value of certain parameters, such as the Higgs mass, directly, which leads to a contribution to the CC that is much larger than the observed value. This prompts an important question: if using the physical mass in the onshell scheme leads to this issue, why not consider an alternative renormalization scheme that could potentially avoid or mitigate the problem? See [21] (and references therein) for a recent work with similar ideas.)

In this spirit, the proposal in [5,6] suggests an alternative approach: rather than using the physical masses directly, one could adopt renormalized mass values that are sufficiently small to avoid causing fine-tuning issues. More specifically, it is suggested that mass values on the order of the temperature might be more appropriate. This would ideally lead to a solution that is less prone to the unnaturalness arising from the onshell renormalization scheme.

The current situation, despite appearing somewhat unnatural with $\Omega_{\Lambda_2} \sim 10^{-8}$, may not necessarily represent an insurmountable obstacle. Instead, it could reflect a situation where the issue might be resolved by adopting a different renormalization scheme. The key feature of this alternative scheme is that the masses are adjusted in such a way that the mass-dependent terms in the potential (as shown in eq. (21)), which were neglected in the previous renormalization scheme applied to the CC problem, are kept small but not negligibly so. This should lead to a slower convergence in the large-temperature expansion since the order of $\frac{m}{T}$, where m denotes the value of the renormalized mass of, say, a Higgs particle, is larger than before. This slow convergence, which was also expected in the proposed CC resolution in [5,6], could, in turn, suggest that the renormalized cosmological constant Λ_{ren} should be set to a value smaller than the observed cosmological constant Λ_{obs} , by several orders of magnitude. This contrasts with the approach used in the CC problem resolution, where the renormalized and observed values were taken to be on the same order.

Such an adjustment would allow for a potential compensation of the deficit through higher-order terms that slowly converge. As a result, the observed value of $\Omega_{\Lambda_2} \sim 10^{-8}$ might not appear as unnatural after all. It is conceivable that higher-order terms in the expansion could shift the one-loop cosmological constant to a value closer to the observed value, thus bridging the gap between the theoretical estimate and the actual observed data.

The situation could also unfold differently on the numerical side. There is a possibility that by repeating the numerical analysis in section 3, and including higher-order terms in the calculation, the optimal value of Ω_{Λ_2} could increase from $\sim 10^{-8}$. In this case, the inclusion of these terms might lead to a larger value for Ω_{Λ_2} , which could help reconcile the numerical result with expectations based on the proposed renormalization scheme. This speculation suggests that the value of Ω_{Λ_2} might not be fixed and could evolve as higher-order corrections are included, offering a potential resolution to the discrepancy.

In conclusion, while the order 10^{-8} might initially seem unnatural, it is possible that the issue could be addressed through the use of an alternative renormalization scheme that adjusts the mass parameters in a way that makes the solution more natural, or that higher-order terms could lead to a more reasonable outcome. Further analysis is required to clarify the situation, and we will address these possibilities in the conclusion.

4 Conclusion

In a flat background, it is a textbook result that finite-temperature effects generate vacuum energy terms. It is natural to expect that this result will be generalized to a curved spacetime, leading to cosmological “constant” terms. This expectation has been verified [7] within the framework of the foliation-based quantization of gravity [8, 9, 11]. The quantum corrections modify, among other things, the cosmological constant term. This work demonstrates the significant impact of the shifted cosmological constant and their implications for the broader set of cosmological parameters. Our analysis suggests that perturbative quantum gravitational effects must be accounted for in periods around recombination, as these effects are not negligible. More specifically, through the introduction of additional parameters, such as Ω_{Λ_2} and Ω_{Λ_3} , we have extended the standard Λ CDM model, offering a more sophisticated approach to fitting cosmological data. By applying the CLASS and utilizing both brute-force scans and machine learning regression techniques, we have demonstrated how the temperature-corrected cosmological parameters can lead to a more accurate fit to the Planck 2018 data. The examination of the 7- and 8- parameter models based on quartic regression has revealed that the presence of a small nonzero value of Ω_{Λ_2} has a significant impact and has shown promise in refining the predictions of the model while preserving its generalizability.

While the results presented here reinforce the utility of finite-T QFT effects in cosmological studies, they also open up avenues for future research. One potential improvement can be seen from the residual plots in Figs. 5 and 6 that display certain patterns for both models, particularly for the 8-variable model. While the residuals remain centered around zero, the spread indicates minor deviations from ideal predictions, especially for higher distance values. These residual patterns suggest that while the models are highly accurate, there is room for improvement in capturing some higher-order non-linearities or interactions present in the data. Various different machine learning techniques, including artificial neural network, have been and are currently being tried. So far, the quartic regression and artificial neural network methods turn out to be best-performing. The result of the artificial neural network [23] shares the same qualitative features as those obtained here. Some complementary aspects, such as feature importance, will be reported therein.

The higher order terms may well play important roles. This anticipation is based on the slow convergence anticipation as was the case in [5, 6] in which the CC problem was tackled. Refining the approach to incorporate higher-order corrections and extending the machine learning methods for enhanced predictive accuracy will thus be important next steps. In particular, it will be worth including one additional parameter, the one associated with the linear temperature term $\sim \frac{1}{a}$, and examine its and its effects on the rest of the parameters.⁸ The exponential growth in the complexity of the parameter space poses substantial challenges that demand supercomputers with greater speed and efficiency. We will report progress on some of these issues elsewhere.

⁸The ellipsis in eq. (23) include the higher-order loop corrections as well as the high-orders terms in $\frac{m}{T}$ expansion. Analyzing the former terms would require even greater effort.

References

- [1] S. Weinberg, “Cosmology,” Oxford university press (2008).
- [2] S. Dodelson and F. Schmidt, ”Modern Cosmology,” Academic Press (2021).
- [3] N. Aghanim *et al.* [Planck], “Planck 2018 results. VI. Cosmological parameters,” *Astron. Astrophys.* **641**, A6 (2020) [erratum: *Astron. Astrophys.* **652**, C4 (2021)] doi:10.1051/0004-6361/201833910 [arXiv:1807.06209 [astro-ph.CO]].
- [4] M. Laine and A. Vuorinen, ”Basics of Thermal Field Theory,” *Lect. Notes Phys.* **925**, 1–281 (2016), doi:10.1007/978-3-319-31933-9 [arXiv:1701.01554 [hep-ph]].
- [5] I. Y. Park, “Cosmological constant as a finite temperature effect,” *Int. J. Mod. Phys. A* **37**, no.27, 2250173 (2022) doi:10.1142/S0217751X22501731 [arXiv:2101.02297 [hep-ph]].
- [6] I. Y. Park, “Quantization of Gravity and Finite Temperature Effects,” *Particles* **4**, no.4, 468-488 (2021) doi:10.3390/particles4040035 [arXiv:2109.01647 [hep-th]].
- [7] I. Y. Park, “Finite-temperature renormalization of Standard Model coupled with gravity, and its implications for cosmology,” [arXiv:2404.07335 [hep-th]].
- [8] I. Y. Park, “Hypersurface foliation approach to renormalization of ADM formulation of gravity,” *Eur. Phys. J. C* **75**, no.9, 459 (2015) doi:10.1140/epjc/s10052-015-3660-x [arXiv:1404.5066 [hep-th]]; “Lagrangian constraints and renormalization of 4D gravity,” *JHEP* **04**, 053 (2015) doi:10.1007/JHEP04(2015)053 [arXiv:1412.1528 [hep-th]]; “One-loop renormalization of a gravity-scalar system,” *Eur. Phys. J. C* **77**, no.5, 337 (2017) doi:10.1140/epjc/s10052-017-4896-4 [arXiv:1606.08384 [hep-th]]; “Revisit of renormalization of Einstein-Maxwell theory at one-loop,” *PTEP* **2021**, no.1, 013B03 (2021) doi:10.1093/ptep/ptaa167 [arXiv:1807.11595 [hep-th]].
- [9] I. Y. Park, *Front. in Phys.* **4**, 25 (2016) doi:10.3389/fphy.2016.00025 [arXiv:1503.02015 [hep-th]].
- [10] E. Witten, “A note on boundary conditions in Euclidean gravity,” *Rev. Math. Phys.* **33**, no.10, 2140004 (2021) doi:10.1142/S0129055X21400043 [arXiv:1805.11559 [hep-th]].
- [11] I. Y. Park, ”Holographic quantization of gravity in a black hole background,” *J. Math. Phys.* **57**, no. 2, 022305 (2016), doi:10.1063/1.4942101 [arXiv:1508.03874 [hep-th]].
- [12] E. Witten, ”A note on the canonical formalism for gravity,” *Adv. Theor. Math. Phys.* **27**, no. 1, 311–380 (2023), doi:10.4310/ATMP.2023.v27.n1.a6 [arXiv:2212.08270 [hep-th]].
- [13] G. Ryskin, “The emergence of cosmic repulsion,” *Astropart. Phys.* **62**, 258-268 (2015) doi:10.1016/j.astropartphys.2014.10.003 [arXiv:1810.07516 [physics.gen-ph]].
- [14] C. Balazs, ”Observable vacuum energy is finite in expanding space,” [arXiv:2203.16753 [gr-qc]].

- [15] D. Blas, J. Lesgourgues and T. Tram, “The Cosmic Linear Anisotropy Solving System (CLASS) II: Approximation schemes,” JCAP **07**, 034 (2011) doi:10.1088/1475-7516/2011/07/034 [arXiv:1104.2933 [astro-ph.CO]].
- [16] CLASS home page: <http://class-code.net/>
- [17] The modified version of CLASS was obtained in collaboration with K. -T. Cho and M. -S. Lee; the code is available at: https://github.com/iparkPSU/modified_CLASS_3.2.1_noleak
- [18] J. Sola, “Cosmological constant and vacuum energy: old and new ideas,” J. Phys. Conf. Ser. **453**, 012015 (2013) doi:10.1088/1742-6596/453/1/012015 [arXiv:1306.1527 [gr-qc]].
- [19] J. Sola Peracaula, “The cosmological constant problem and running vacuum in the expanding universe,” Phil. Trans. Roy. Soc. Lond. A **380**, 20210182 (2022) doi:10.1098/rsta.2021.0182 [arXiv:2203.13757 [gr-qc]].
- [20] C. Moreno-Pulido, J. Sola Peracaula and S. Cheraghchi, “Running vacuum in QFT in FLRW spacetime: the dynamics of $\rho_{\text{vac}}(H)$ from the quantized matter fields,” Eur. Phys. J. C **83**, no.7, 637 (2023) doi:10.1140/epjc/s10052-023-11772-9 [arXiv:2301.05205 [gr-qc]].
- [21] Y. Ageeva, P. Petrov, and M. Shaposhnikov, ”Non-renormalizable theories and finite formulation of QFT,” [arXiv:2409.15036 [hep-th]].
- [22] V. Poulin, T. L. Smith, T. Karwal and M. Kamionkowski, “Early Dark Energy Can Resolve The Hubble Tension,” Phys. Rev. Lett. **122**, no.22, 221301 (2019) doi:10.1103/PhysRevLett.122.221301 [arXiv:1811.04083 [astro-ph.CO]].
- [23] A. Hatefi, E. Hatefi, and I. Y. Park, manuscript in preparation.